

# Inferring Concepts from Noisy Examples in Hopfield-like Neural Networks

Marco Benedetti

*Università Bocconi, Milan, Italy*

Giulia Fischetti

*Ca' Foscari Università Venezia, ZHAW Switzerland*

Enzo Marinari

*Università di Roma La Sapienza, Rome, Italy*

Gleb Oshanin, Victor Dotsenko

*Sorbonne Université, CNRS, Laboratoire de Physique Théorique de la Matière Condensée, Paris, France*

We study a variant of the pseudo-inverse learning rule for Hopfield-like Neural Networks, which allows the network to infer archetypal concepts on the basis of a limited number of examples. The mean-field replica theory for this model reveals how this generalization ability is mediated by a multitude of states, with diverse thermodynamic properties, coexisting with the standard Hopfield ones. They appear and vanish through smooth transitions or discontinuous jumps and, interestingly, show much stronger Replica Symmetry Breaking (RSB) effects than the standard Hopfield model, as captured by our 1RSB analysis. Our results, in excellent agreement with numerical simulations, provide deeper insight into the interplay between memory storage and generalization in attractor neural networks.

## I. Introduction

The development of models and tools from theoretical physics has greatly contributed to our understanding of neural computation and memory storage. Among these, attractor neural networks have emerged as particularly important frameworks for understanding how the brain might store and retrieve information [1–3]. The Hopfield model [4] represents one of the most influential examples of such networks, consisting of binary neurons connected through symmetric pairwise interactions. In this framework, memory patterns are stored as attracting fixed points of the neural dynamics, enabling associative memory retrieval from partial or corrupted inputs. The synaptic weights are typically determined by the Hebbian learning rule [5], which provides local learning based on correlations between neural activities. In the context of Attractor Neural Networks, the ability to generalize can be understood as a synthesis process, where the learning rule extracts useful information about general concepts (Archetypes) on the basis of examples [6]. An Attractor Neural Networks is said to be generalizing if it builds attractors more correlated to the archetype than to the individual examples provided for it. In this setting, the examples pertaining to the same archetype display strong correlations, and the mutual overlaps between examples act as interference noise, dramatically reducing storage capacity and retrieval quality in the standard Hopfield model. This has motivated the development of alternative learning algorithms, most notably the pseudo-inverse learning rule [7, 8], which can perfectly store any set of linearly independent patterns up to the theoretical limit of one pattern per neuron. While the pseudo-inverse rule eliminates interference noise, it suffers from two crucial

drawbacks: first, it is fundamentally non-local, requiring global knowledge of all patterns to determine each synaptic weight. This contradicts biological plausibility and makes the learning process computationally expensive, as adding new patterns requires recalculating the entire weight matrix. Second, the pseudo-inverse is too effective in building separate attractors for each example, rather than extracting information about the archetype, thus hindering generalization. This has also been noted in [9, 10], where a parametric procedure inspired by Hebbian Unlearning [11–14] was devised, interpolating between Hebbian Learning and pseudo-inverse learning to promote generalization over overfitting in pseudo-inverse based learning rules.

In this paper, we propose a novel approach that combines accurate pattern storage for hierarchically correlated patterns and strong ability to generalize from limited number of examples. Unlike in the standard pseudo-inverse rule, in our scheme correlations are dealt with by means of the expected correlation structure of the dataset, rather than the empirical one. Hence, our learning mechanism maintains locality of learning and allows for incremental learning. This simple modification has profound consequences, increasing the generalization capabilities of the model, and leads to a rich phase behavior, where multiple solution types coexist, corresponding to different generalization strategies.

The paper is organized as follows: section II provides the details of our model; section III contains our main results, i.e. the study of the multiple generalizing thermodynamic states of the network, within a Replica Symmetric Mean Field analysis; section V contains the comparison between analytical predictions and simulations, as well as comments on Replica Symmetry Breaking effects.

## II. Model Description

We consider a fully connected network of  $N$  binary neurons  $\{\sigma_i = \pm 1\}$  ( $i = 1, 2, \dots, N$ ) described by the Hamiltonian:

$$H[\sigma, J] = -\frac{1}{2} \sum_{j \neq i}^N J_{ij} \sigma_i \sigma_j. \quad (1)$$

The coupling matrix is a variant of the pseudo-inverse learning rule, namely

$$J_{ij} = \frac{1}{N} \sum_{\mu, \nu}^P \overline{C_{\mu\nu}^{-1}} \xi_i^\mu \xi_j^\nu \quad (2)$$

where  $\overline{C_{\mu\nu}} = \overline{\xi_i^\mu \xi_i^\nu}$  and  $\{\xi_i^\mu = \pm 1\}$  are the examples. In this paper, we will be focusing on a 2-level hierarchy of correlated examples, based on sampling a number  $P/K$  of  $N$  dimensional i.i.d. configurations (the archetypes), and then corrupting them with multiplicative noise, to get from each a number  $K$  of examples. In formulas  $\xi_i^{\alpha_1 \alpha_2} = \eta_i^{\alpha_1} \zeta_i^{\alpha_1 \alpha_2}$ , where  $\eta_i^{\alpha_1}$  represents the archetype and  $\zeta_i^{\alpha_1 \alpha_2}$  introduces intra-family variations. We are going to consider the following statistics for the examples:

$$P(\eta_i^{\alpha_1} = x) = \frac{1}{2} (\delta(x-1) + \delta(x+1)), \quad (3)$$

$$P(\zeta_i^{\alpha_1 \alpha_2} = x) = \frac{1+\rho}{2} \delta(x-1) + \frac{1-\rho}{2} \delta(x+1). \quad (4)$$

Here  $\alpha_1 = 1, \dots, P/K$  labels the families and  $\alpha_2 = 1, \dots, K$  labels patterns within each family. The parameter  $\rho$  sets the amount of noise driving examples apart from archetypes. It follows that  $\overline{C_{\mu\nu}}$  has a block diagonal structure: within each family, patterns have overlap  $q = \rho^2$ , while patterns from different families are uncorrelated.

Notice the difference between this prescription and the pseudo-inverse learning rule, which is based on the empirical correlation of the examples  $C_{\mu\nu} = 1/N \sum_i \xi_i^\mu \xi_i^\nu$ . While the pseudo-inverse learning rule leverages the detailed knowledge of the random examples presented to the network, our prescription is only aware of their average correlation structure. This has a strong impact on the performance of the model, since the pseudo-inverse learning rule is extremely effective in stabilizing individual examples, and leads to a phenomenology identical to that of the Hopfield model, namely attractors corresponding to the examples, rather than the archetypes. In other words, a form of overfitting. We will see how eq. (2) allows the network to create other types of attractors, closer to the archetypes  $\eta^{\alpha_1}$  than to the individual examples  $\xi^{\alpha_1 \alpha_2}$ , enhancing the generalization capabilities of the model.

## III. Replica Symmetric Mean-Field Theory

The Replica Symmetric (RS) mean-field theory analysis of the model is similar to that of the standard Hopfield model. The order parameters of the model are  $m_{\alpha_1 \alpha_2} := N^{-1} \mathbb{E}[\sum_i \xi_i^{\alpha_1 \alpha_2} \langle \sigma_i \rangle]$ ,  $r := \alpha^{-1} \mathbb{E}[\sum_{\alpha_1 \alpha_2} (m_{\alpha_1 \alpha_2})^2]$  and  $Q := N^{-1} \sum_i \langle \sigma_i \rangle^2$ , and are determined by minimizing a Free Energy function, see section A. The Free Energy of the model is most naturally expressed in terms of  $x_{\alpha_1 \alpha_2}$  variables, dual to the overlaps as specified by

$$m_{\alpha_1 \alpha_2} = (1-q) x_{\alpha_1 \alpha_2} + q \left( \sum_{\alpha'_2=1}^K x_{\alpha_1 \alpha'_2} \right). \quad (5)$$

In addition, we will keep track of the overlap between the network state and the archetypes,  $O^{\alpha_1} = N^{-1} \mathbb{E}[\sum_i \eta_i^{\alpha_1} \langle \sigma_i \rangle]$ . When  $O^{\alpha_1} > m_{\alpha_1 \alpha_2}$ , we will say that the Network is “generalizing”, i.e. it is extracting from the examples information about the archetype, rather than focusing on the individual examples.

### A. Ansatz on saddle point solutions

The model exhibits only solutions where the  $x$  variables are non-zero within a single archetype class  $\alpha_1$ , and we will therefore suppress the archetype index  $\alpha_1$  in what follows. Furthermore, we will assume that  $x_2 = x_3 = \dots = x_K$  while  $x_1$  is allowed to have a different value. This implies that  $m_2 = m_3 = \dots = m_K$ . As we will see, this ansatz captures the essential physics while remaining tractable. The physical interpretation is that our description allows the system to single out a specific example  $\alpha_2 = 1$ , while all others are treated in a completely symmetric fashion. MF equations and details about their solutions are reported in section A and section C. Within this ansatz, one finds the standard Hopfield model solutions, where  $x_2 = 0$  and:  $x_1 (= m_1) = 0, Q = 0, \rho = 0$  for the paramagnetic solution;  $x_1 (= m_1) = 0, Q \neq 0, r \neq 0$  for the spin-glass solution;  $x_1 (= m_1) \neq 0, Q \neq 0, r \neq 0$  for the Hopfield retrieval solution.

Alongside these solutions, we find a novel and articulate set of solutions, which are “generalizing”, in the sense that  $O > m_1, m_2$ . Namely:

- Fully Symmetric (FS) solution  $m_1 = m_2, (x_1 = x_2) Q \neq 0, r \neq 0$ : the network generalizes without any bias towards any of the examples.
- Class Representant (CR) solution  $m_1 > m_2 (x_1 > x_2), Q \neq 0, r \neq 0$ : the network shows a preference towards one of the examples corresponding to the archetype;
- Outlier Excluding (OE) solution  $m_1 < m_2 (x_1 < x_2), Q \neq 0, r \neq 0$ : a ‘leave-one-out’ solution generalization mechanism, where the network aligns

symmetrically and preferentially towards  $K - 1$  examples, while one is regarded as an outlier;

This reveals how the network not only balances between memorizing specific examples and inferring archetypes, as noted for similar learning rules in [9, 10], but also generalizes according to a multitude of strategies, corresponding to states with different thermodynamic properties. All generalizing solutions are metastable states of the system, while the lowest free energy states are the same as in the Hopfield model as  $\alpha$  and  $T$  vary. Still, analogously to the Hopfield model, metastable states can perform neural computations, as they are surrounded by extensive free energy barriers, and escape times to the thermodynamically dominant state are exponential in  $N$ .

#### IV. Analytical Characterization of the Generalizing states

The three solutions  $x_2 = 0$ , which are present also in the standard Hopfield model, are described by the same phase diagram, described in [2]. Hence, in the following we will only concentrate on the novel  $x_2 > 0$  solutions, where generalization occurs. The phenomenology associated with the three kinds of solutions is very rich, as can be appreciated from the zero temperature picture in the RS approximation Figure 1. It goes as follows: the FS solution exists in an interval  $\alpha_{min}^{fs} < \alpha < \alpha_{max}^{fs}$ ; the CR solution exists in the interval  $0 < \alpha < \alpha_{max}^{cr}$ ; the OE solution exists in the intervals  $0 < \alpha < \alpha_{max1}^{oe}$  and  $\alpha_{min}^{oe} < \alpha < \alpha_{max2}^{oe}$ . Varying the values of  $T$ ,  $r$  and  $K$ , one can change the values of these thresholds. Broadly speaking, increasing the quality of the dataset leads to a more dominant FS. Specifically, the amplitude of the interval  $\alpha_{min}^{fs} < \alpha < \alpha_{max}^{fs}$  increases with both  $K$  and dataset quality, and fills the whole area under the Hopfield transition line when  $K \rightarrow \infty$  or  $r \rightarrow 1$ . The order parameters associated with this solution coincide with the Hopfield ones in this limit. Both  $\alpha_{max}^{cr}$  and  $\alpha_{max1}^{oe}$  reduce by increasing  $r$  or  $K$ , and  $\alpha_{min}^{oe}$  increases by increasing  $r$  or  $K$ . In all cases, we found that  $0 < \alpha_{max}^{cr} < \alpha_{max1}^{oe}$  and  $\alpha_{max}^{fs} = \alpha_{min}^{oe}$ . The behavior of the solutions at their critical point is also various: at  $\alpha_{max2}^{oe}$  the OE solution disappears discontinuously. At  $\alpha_{max1}^{oe}$  and  $\alpha_{max}^{cr}$  the OE and CR solutions can, depending on  $K$  and dataset quality  $\rho$ , either disappear discontinuously, or merge continuously with the FS solution. Figure 1 shows the RS bifurcation diagram at zero temperature for  $K = 4$  and  $\rho = 0.75, 0.8$ . The diagram displays the overlaps  $m_1$  (with the singled-out pattern) and  $m_2$  (with other patterns in the family) as functions of the load parameter  $\alpha$ . Different solution types are color-coded, revealing complex bifurcation structure with multiple solution branches coexisting in certain parameter regions, with smooth transitions between some phases and discontinuous jumps between others.

The temperature-load parameter phase diagrams provide a complete picture of the system's behavior. Fig-

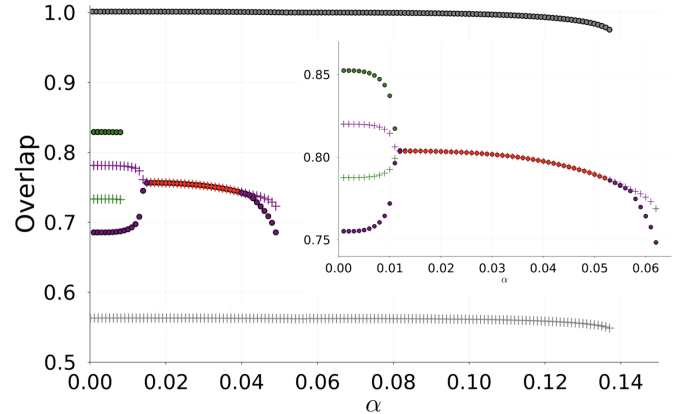


FIG. 1: Overlap bifurcation diagrams at  $T = 0$  and  $K = 4$ . Main figure shows results for  $\rho = 0.75$ , the inset for  $\rho = 0.8$ . The diagrams show different RS MFT solution types characterized by overlaps  $m_1$  (dots) and  $m_2$  (crosses) as a function of  $\alpha$ . Red identifies the FS solution, green the CR solution, purple the OE solution.

ure 2 shows the RS phase boundaries for  $K = 4$  at two different correlation strengths:  $\rho = 0.75$  and  $\rho = 0.8$ .

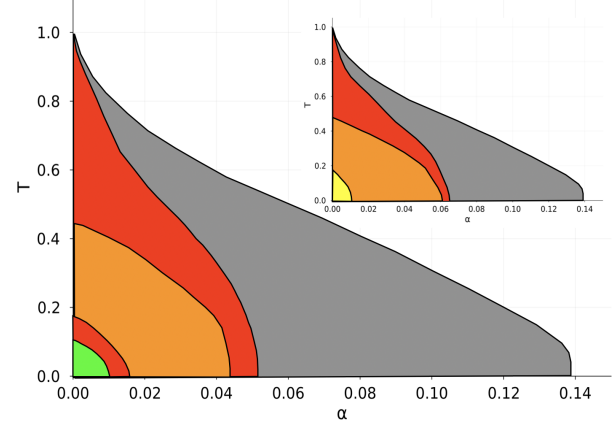


FIG. 2: Phase boundaries in the temperature-load parameter space for  $K = 4$  examples per archetype. Main figure shows results for dataset-quality  $\rho = 0.75$  while the inset for  $\rho = 0.80$ . Red indicates where only the OE exists, Orange indicates where only the FS solution exists, yellow indicates where the CR and the OE solution coexists.

#### V. Comparison with Numerical Results and 1RSB

We performed numerical simulations to validate our  $T = 0$  mean-field predictions. We did not compare with simulations the finite temperature picture, as all generalizing solutions are metastable states of the system, and

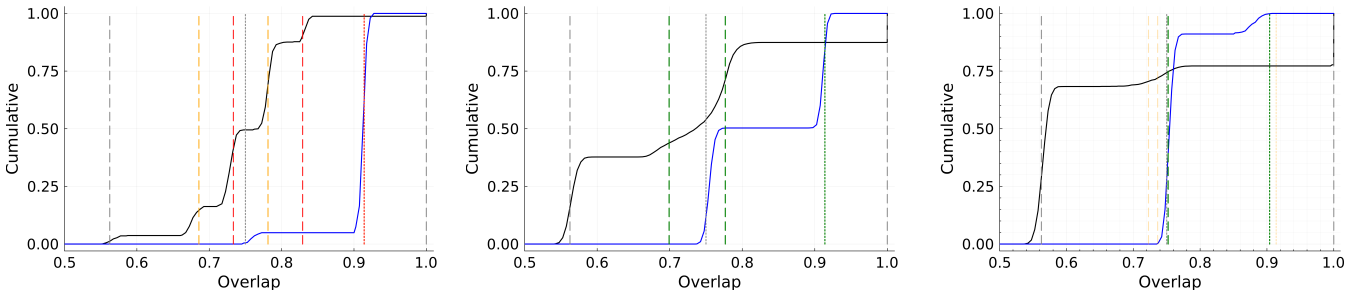


FIG. 3: Comparison between 1RSB mean-field theory predictions and simulations for zero temperature overlap cumulative distribution function at load parameter  $\alpha = 0.005$  (left);  $\alpha = 0.015$  (center);  $\alpha = 0.045$  (right). Other

parameters are:  $N = 8192$ ,  $K = 4$  hierarchy levels, correlation strength  $\rho = 0.75$ . Full lines show cumulative distribution functions of overlaps with examples (black lines) and archetype (blue lines). MFT predictions are shown as vertical lines, dashed for overlaps with examples, dotted for overlaps with the archetype. Orange corresponds to the OE solution, red to the CR solution, green to the FS solution, gray to the Hopfield solution. In the right panel a very transparent shade indicates the RS estimate, showcasing how 1RSB improves the matching with simulations.

a thermalized system would always show only the Hopfield solution. Simulations were conducted on networks up to  $N = 8192$  spins, using zero temperature Monte Carlo dynamics. The network is initialized to one of the archetypes and relaxed to a fixed point. We then measure overlaps with both the archetype and all examples within that archetype family, yielding  $K + 1$  overlaps per simulation (the  $K$  example overlaps are collected together). From these overlap distributions, we construct cumulative distribution function (CDF) functions where peaks appear as sharp rises. The step heights reflect relative frequencies and are strongly dependent on initialization strategy, while step locations are physical and comparable to MFT predictions. Figure 3 displays experimental CDFs of examples (black lines) and archetypes (blue lines) overlaps at different values of the load parameter  $\alpha$ . Mean-field theory predictions for the examples and archetype overlaps are shown as dashed and dotted vertical lines respectively. The color-coding identifies different types of solutions. Notice that different solution types have extremely similar values of archetype overlap, so that the whole zoology of solutions would go undetected, if one did not measure the example-overlaps.

Generally speaking, RS MFT gives accurate predictions of the intricate overlap structures displayed by the simulations. While this agreement is essentially perfect for low values of alpha, it degrades and becomes only qualitative as alpha is increased, particularly close to the transitions  $\alpha$ . The 1RSB MFT (see section C) predictions are found to always improve the agreement between theory and simulations. As a rule, 1RSB solutions follow the same qualitative patterns highlighted in section IV, with the difference that all solutions survive to higher values of  $\alpha$ . This effect, present also in the standard Hopfield model, here is more relevant, with the zero temperature critical loads being up to 30% higher than the RS ones. As in the Hopfield model, the RSB becomes relevant only for very low values of  $T \sim 0.02$ , and leaves the higher temperature phase diagram unchanged.

## VI. Conclusions

We have analyzed a novel neural network model, using a modified pseudo-inverse learning rule based on theoretical rather than empirical pattern correlations. This formulation, preserving both biological plausibility and computational efficiency, allows the network to generalize, extracting information about archetypes from a limited number of noisy examples. Our RS and 1RSB mean-field analysis reveals a rich solution landscape. We identify six distinct classes of solutions, three of which have generalization properties, meaning that they are characterized by an archetype overlap larger than the overlap with the individual samples. The critical capacities depend on the number of examples per archetype  $K$  and the dataset quality  $r$ , with stronger correlations extending the domain of the fully symmetric solution. Interestingly, different solution types exhibit extremely similar archetype overlaps, meaning that the rich solution structure would remain hidden without careful measurement of individual pattern overlaps. The theoretical predictions in the 1RSB approximation are in excellent agreement to zero temperature Monte Carlo simulations across wide parameter ranges. Replica symmetry breaking effects are more pronounced than in standard Hopfield models, with the RS zero temperature critical loads being up to 30% lower than the 1RSB ones.

Our work demonstrates that subtle modifications in how neural network learning rules can lead to qualitatively new behaviors, effectively bridging the fundamental tension between memory storage and generalization. This opens promising avenues for both theoretical understanding of neural computation and practical applications in machine learning and computational neuroscience. Extending the hierarchical pattern structure beyond two levels in the spirit of [15, 16] presents an intriguing challenge, and may further increase replica symmetry breaking effects, potentially revealing even richer phase behavior.

---

[1] W. A. Little, The existence of persistent states in the brain, *Mathematical Biosciences* **19**, 101 (1974).

[2] D. J. Amit, H. Gutfreund, and H. Sompolinsky, Spin-glass models of neural networks, *Physical Review A* **32**, 1007 (1985).

[3] D. J. Amit, *Modeling Brain Function: The World of Attractor Neural Networks* (Cambridge University Press, Cambridge, 1989).

[4] J. J. Hopfield, Neural networks and physical systems with emergent collective computational abilities., *Proceedings of the National Academy of Sciences* **79**, 2554 (1982).

[5] D. O. Hebb, *Organization of behavior*. New York: Wiley, 1949, pp. 335, \$4.00, *Journal of Clinical Psychology* **6**, 307 (1950).

[6] E. Agliari, F. Alemanno, A. Barra, and G. De Marzo, The emergence of a concept in shallow neural networks, *Neural Networks* **148**, 232 (2022).

[7] L. Personnaz, I. Guyon, and G. Dreyfus, Information storage and retrieval in spin-glass like neural networks, *Journal de Physique Lettres* **46**, 359 (1985).

[8] I. Kanter and H. Sompolinsky, Associative recall of memory without errors, *Physical Review A* **35**, 380 (1987).

[9] M. Aquaro, F. Alemanno, I. Kanter, F. Durante, E. Agliari, and A. Barra, Recurrent neural networks that generalize from examples and optimize by dreaming (2022), arXiv:2204.07954 [cond-mat].

[10] E. Agliari, F. Alemanno, M. Aquaro, A. Barra, F. Durante, and I. Kanter, Hebbian dreaming for small datasets, *Neural Networks* **173**, 106174 (2024).

[11] J. J. Hopfield, D. I. Feinstein, and R. G. Palmer, ‘Unlearning’ has a stabilizing effect in collective memories, *Nature* **304**, 158 (1983).

[12] J. L. Van Hemmen, L. B. Ioffe, R. Kühn, and M. Vaas, Increasing the efficiency of a neural network through unlearning, *Physica A: Statistical Mechanics and its Applications* **163**, 386 (1990).

[13] M. Benedetti, E. Ventura, E. Marinari, G. Ruocco, and F. Zamponi, Supervised perceptron learning vs unsupervised Hebbian unlearning: Approaching optimal memory retrieval in Hopfield-like networks, *The Journal of Chemical Physics* **156**, 104107 (2022).

[14] M. Benedetti, L. Carillo, E. Marinari, and M. Mézard, Eigenvector dreaming, *Journal of Statistical Mechanics: Theory and Experiment* **2024**, 013302 (2024).

[15] V. Dotsenko, Hierarchical model of memory, *Physica A: Statistical Mechanics and its Applications* **140**, 410 (1986).

[16] N. Parga and M. A. Virasoro, The ultrametric organization of memories in a neural network, *Journal de Physique* **47**, 1857 (1986).

[17] A. Crisanti, D. J. Amit, and H. Gutfreund, Saturation Level of the Hopfield Model for Neural Network, *Europhysics Letters* **2**, 337 (1986).

[18] H. Steffan and R. Kühn, Replica symmetry breaking in attractor neural network models, *Zeitschrift für Physik B Condensed Matter* **95**, 249 (1994).

### A. Finite Temperature Replica Symmetric Free Energy

The derivation of the Replica Symmetric Free Energy follows standard techniques in the theory of disordered systems, and is very similar to the standard Hopfield model (see [2]). The partition function of the system reads

$$Z = \sum_{\{\sigma\}} \exp \left\{ \frac{1}{2} \beta \sum_{i,j}^N J_{ij} \sigma_i \sigma_j \right\} = \sum_{\{\sigma\}=\pm 1} \exp \left\{ \frac{\beta}{2N} \sum_{i,j}^N \sum_{\mu,\nu}^P \overline{C_{\mu\nu}^{-1}} \xi_i^\mu \xi_j^\nu \sigma_i \sigma_j \right\} \quad (\text{A1})$$

Performing a Hubbard-Stratonovich transformation to linearize in the  $\sigma$  variables leads to

$$Z = \prod_{\mu=1}^P \left( \int_{-\infty}^{\infty} dx_\mu \right) \sum_{\{\sigma\}=\pm 1} \exp \{-\beta H[\mathbf{X}; \boldsymbol{\sigma}]\}; \quad H[\mathbf{X}; \boldsymbol{\sigma}; \boldsymbol{\xi}] = \frac{1}{2} N \sum_{\mu,\nu}^P \overline{C_{\mu\nu}} x_\mu x_\nu + \sum_{\mu}^P \sum_i^N \sigma_i \xi_i^\mu x_\mu. \quad (\text{A2})$$

Introducing the detailed structure of the  $\overline{C_{\mu\nu}}$  matrix and of the patterns  $\xi_i^{\alpha_1 \alpha_2} = \eta_i^{\alpha_1} \zeta_i^{\alpha_1 \alpha_2}$  leads to

$$H[\mathbf{X}; \boldsymbol{\sigma}; \boldsymbol{\eta}; \boldsymbol{\zeta}] = \frac{1}{2} N (1-q) \sum_{\alpha_1=1}^{P/K} \sum_{\alpha_2=1}^K x_{\alpha_1 \alpha_2}^2 + \frac{1}{2} N q \sum_{\alpha_1=1}^{P/K} \left( \sum_{\alpha_2=1}^K x_{\alpha_1 \alpha_2} \right)^2 + \sum_{\alpha_1=1}^{P/K} \sum_{\alpha_2=1}^K \sum_i^N \sigma_i \eta_i^{\alpha_1} \zeta_i^{\alpha_1 \alpha_2} x_{\alpha_1 \alpha_2} \quad (\text{A3})$$

where  $q = \rho^2$  is the overlap between examples pertaining to the same archetype. In the spirit of replica calculations, we aim at computing averages of powers of  $Z$ , and obtain the quenched Free Energy through

$$\langle \log(Z) \rangle = \lim_{n \rightarrow 0} \frac{\langle Z^n \rangle - 1}{n} \quad (\text{A4})$$

The average values of the  $x$  variables are related to the overlaps between spins and examples, as in eq. (5). As in the Hopfield model, we assume that only a subset of such variables are with high probability finite in the limit  $N \rightarrow \infty$ , say those with index  $\alpha_1 = 1$ . Rescaling the other variables  $x_{\alpha_1 \alpha_2} \leftarrow 1/\sqrt{N} x_{\alpha_1 \alpha_2}$  for  $\alpha_1 > 1$ , the replicated average partition function reads

$$\begin{aligned} \langle Z^n \rangle &\propto \prod_{\alpha=1}^K \prod_{a=1}^n \left( \int_{-\infty}^{+\infty} dx_\alpha^a \right) \prod_{i=1}^N \prod_{a=1}^n \left( \sum_{\sigma_i^a = \pm 1} \right) \prod_{i=1}^N \left[ \sum_{\eta_i^1 = \pm 1} \prod_{\alpha=1}^K \left( \sum_{\zeta_i^\alpha = \pm 1} P(\zeta_i^\alpha) \right) \right] \\ &\times \exp \left\{ -\frac{1}{2} \beta N (1-q) \sum_{\alpha=1}^K \sum_{a=1}^n (x_\alpha^a)^2 - \frac{1}{2} \beta N q \sum_{a=1}^n \left( \sum_{\alpha=1}^K x_\alpha^a \right)^2 + \beta \sum_{\alpha=1}^K \sum_{i=1}^N \sum_{a=1}^n \sigma_i^a \eta_i^1 \zeta_i^\alpha x_\alpha^a \right\} \tilde{Z}_n[\sigma]. \end{aligned} \quad (\text{A5})$$

where  $x_\alpha \equiv x_{1\alpha}$ ,  $\zeta_i^\alpha \equiv \zeta_i^{1\alpha}$ , and  $\tilde{Z}_n[\sigma]$  is

$$\begin{aligned} \tilde{Z}_n[\sigma] &= \prod_{\alpha_1=2}^{P/K} \prod_{\alpha_2=1}^K \prod_{a=1}^n \left( \int_{-\infty}^{+\infty} dx_{\alpha_1 \alpha_2}^a \right) \exp \left\{ -\frac{1}{2} \beta (1-q) \sum_{\alpha_1=2}^{P/K} \sum_{\alpha_2=1}^K \sum_{a=1}^n (x_{\alpha_1 \alpha_2}^a)^2 - \frac{1}{2} \beta q \sum_{\alpha_1=2}^{P/K} \sum_{a=1}^n \left( \sum_{\alpha_2=1}^K x_{\alpha_1 \alpha_2}^a \right)^2 \right\} \\ &\times \prod_{i=1}^N \prod_{\alpha_1=2}^{P/K} \left[ \sum_{\eta_i^{\alpha_1} = \pm 1} \prod_{\alpha_2=1}^K \left( \sum_{\zeta_i^{\alpha_1 \alpha_2} = \pm 1} P(\zeta_i^{\alpha_1 \alpha_2}) \times \exp \left\{ \frac{\beta}{\sqrt{N}} \eta_i^{\alpha_1} \zeta_i^{\alpha_1 \alpha_2} \sum_{a=1}^n \sigma_i^a x_{\alpha_1 \alpha_2}^a \right\} \right) \right] \end{aligned} \quad (\text{A6})$$

Expanding the last line of eq. (A6) to leading order in  $N$  and using the integral representation of the Dirac  $\delta$

function to enforce the definition  $Q_{ab} = \frac{1}{N} \sum_{i=1}^N \sigma_i^a \sigma_i^b$  we get

$$\begin{aligned} \tilde{Z}_n[\sigma] \propto & \prod_{a \neq b}^n \left( \int_{-\infty}^{+\infty} ds_{ab} \int_{-\infty}^{+\infty} dQ_{ab} \right) \exp \left\{ iN \sum_{a \neq b}^n s_{ab} Q_{ab} - i \sum_{a \neq b}^n s_{ab} \sum_{i=1}^N \sigma_i^a \sigma_i^b \right\} \times \\ & \times \left[ \prod_{\alpha=1}^K \prod_{a=1}^n \left( \int_{-\infty}^{+\infty} dx_{\alpha}^a \right) \exp \left\{ -\frac{1}{2} \beta(1-\beta)(1-q) \sum_{\alpha=1}^K \sum_{a=1}^n (x_{\alpha}^a)^2 - \frac{1}{2} \beta(1-\beta)q \sum_{a=1}^n \left( \sum_{\alpha=1}^K x_{\alpha}^a \right)^2 + \right. \right. \\ & \left. \left. + \frac{1}{2} \beta^2(1-q) \sum_{a \neq b}^n Q_{ab} \sum_{\alpha=1}^K x_{\alpha}^a x_{\alpha}^b + \frac{1}{2} \beta^2 q \sum_{a \neq b}^n Q_{ab} \left( \sum_{\alpha=1}^K x_{\alpha}^a \right) \left( \sum_{\alpha'=1}^K x_{\alpha'}^b \right) \right\} \right]^{(\frac{P}{K}-1)}. \end{aligned} \quad (\text{A7})$$

Finally, we substitute Eq. A7 into Eq. A5, obtaining

$$\begin{aligned} \langle Z^n \rangle \propto & \prod_{a \neq b}^n \left( \int_{-\infty}^{+\infty} ds_{ab} \int_{-\infty}^{+\infty} dQ_{ab} \right) \prod_{\alpha=1}^K \prod_{a=1}^n \left( \int_{-\infty}^{+\infty} dx_{\alpha}^a \right) \times \\ & \times \exp \left\{ -\frac{1}{2} \beta N (1-q) \sum_{\alpha=1}^K \sum_{a=1}^n (x_{\alpha}^a)^2 - \frac{1}{2} \beta N q \sum_{a=1}^n \left( \sum_{\alpha=1}^K x_{\alpha}^a \right)^2 + iN \sum_{a \neq b}^n s_{ab} Q_{ab} + \right. \\ & \left. + \frac{\alpha N}{K} \ln [I_{n,K}(Q)] + N \ln [\mathcal{Z}(s)] \right\}, \end{aligned} \quad (\text{A8})$$

where

$$\begin{aligned} I_{n,K}(Q) = & \prod_{\alpha=1}^K \prod_{a=1}^n \left( \int_{-\infty}^{+\infty} dy_{\alpha}^a \right) \exp \left\{ -\frac{1}{2} \beta(1-\beta)(1-q) \sum_{\alpha=1}^K \sum_{a=1}^n (y_{\alpha}^a)^2 - \frac{1}{2} \beta(1-\beta)q \sum_{a=1}^n \left( \sum_{\alpha=1}^K y_{\alpha}^a \right)^2 + \right. \\ & \left. + \frac{1}{2} \beta^2(1-q) \sum_{a \neq b}^n Q_{ab} \sum_{\alpha=1}^K y_{\alpha}^a y_{\alpha}^b + \frac{1}{2} \beta^2 q \sum_{a \neq b}^n Q_{ab} \left( \sum_{\alpha=1}^K y_{\alpha}^a \right) \left( \sum_{\alpha'=1}^K y_{\alpha'}^b \right) \right\} \end{aligned} \quad (\text{A9})$$

and

$$\mathcal{Z}(s) = \prod_{a=1}^n \left( \sum_{\sigma_a=\pm 1} \right) \prod_{\alpha=1}^K \left( \sum_{\zeta^{\alpha}=\pm 1} P(\zeta^{\alpha}) \right) \sum_{\eta=\pm 1} \exp \left\{ \beta \sum_{\alpha=1}^K \sum_{a=1}^n \sigma_a \eta \zeta^{\alpha} x_{\alpha}^a - i \sum_{a \neq b}^n s_{ab} \sigma_a \sigma_b \right\}. \quad (\text{A10})$$

All integrals can be evaluated to leading order using the saddle point method. The replica symmetric approximation states that the saddle-point values of the order parameter matrices  $Q_{ab}$  and  $s_{ab}$  as well as the components of the replica vector  $x_{\alpha}^a$  do not depend on the replica indices, namely,  $Q_{a \neq b} = Q$ ,  $s_{a \neq b} = s$  and  $x_{\alpha}^a = x_{\alpha}$ . The saddle point value of the parameter  $s$  is pure imaginary, therefore it is convenient to rewrite it as  $s = \frac{i}{2} \alpha \beta^2 r$  introducing the new parameter  $r$ . With this definition, one obtains

$$\langle Z^n \rangle \propto \exp \left\{ -\beta n N F[Q, r, x_1, \dots, x_K] \right\} \quad (\text{A11})$$

with

$$\begin{aligned} F[Q, r, x_1, \dots, x_K] = & \frac{1}{2} (1-q) \sum_{\alpha=1}^K (x_{\alpha})^2 + \frac{1}{2} q \left( \sum_{\alpha=1}^K x_{\alpha} \right)^2 + \frac{1}{2} \alpha \beta r (1-Q) \\ & - \frac{\alpha}{\beta n K} \ln [\tilde{I}_{n,K}(Q)] - \frac{1}{\beta n} \ln [\tilde{\mathcal{Z}}_{n,K}(r; \{x_{\alpha}\})] \end{aligned} \quad (\text{A12})$$

where the values of the parameters  $Q$ ,  $r$  and  $x_1, \dots, x_K$  are defined by the saddle-point equations  $\partial F / \partial Q = 0$ ;  $\partial F / \partial r =$

0 and  $\partial F/\partial x_\alpha = 0$  ( $\alpha = 1, 2, \dots, K$ ), and

$$\tilde{\mathcal{Z}}_{n,K}(r; \{x_\alpha\}) = \prod_{a=1}^n \left( \sum_{\sigma_a=\pm 1} \right) \prod_{\alpha=1}^K \left( \sum_{\zeta^\alpha=\pm 1} P(\zeta^\alpha) \right) \sum_{\eta=\pm 1} \exp \left\{ \beta \sum_{\alpha=1}^K \sum_{a=1}^n \sigma_a \eta \zeta^\alpha x_\alpha + \frac{1}{2} \alpha \beta^2 r \left( \sum_{a=1}^n \sigma_a \right)^2 \right\},$$

$$\tilde{I}_{n,K}(Q) = (2\pi)^{\frac{1}{2}Kn} A^{-Kn/2} (1-nb)^{-(K-1)/2} (1+Kc)^{-(n-1)/2} (1-nb+Kc)^{-1/2} \left[ 1 - \frac{Knd(1+Kc-nb-Knbc)}{(1-nb)(1+Kc)(1-nb+Kc)} \right]^{-1/2}.$$

Above, we introduced symbols

$$A = \beta(1-q)[1 - \beta(1-Q)]$$

$$b = \frac{\beta Q}{1 - \beta(1-Q)}$$

$$c = \frac{q}{1-q}$$

$$d = \frac{q\beta Q}{(1-q)(1-\beta(1-Q))}$$

Introducing the Gaussian measure  $\mathcal{D}z := \exp(-z^2/2)dz$ , in the limit  $n \rightarrow 0$ , we obtain

$$\lim_{n \rightarrow 0} \frac{1}{n} \ln [\tilde{\mathcal{Z}}_{n,K}(r; \{x_\alpha\})] = \int \mathcal{D}z \left\langle \left\langle \ln \left[ 2 \cosh \left[ \beta \left( \sum_{\alpha=1}^K \zeta^\alpha x_\alpha + \sqrt{\alpha r} z \right) \right] \right] \right\rangle \right\rangle_\zeta; \quad (\text{A13})$$

$$\lim_{n \rightarrow 0} \frac{1}{n} \ln [\tilde{I}_{n,K}(Q)] = -\frac{1}{2} K \left[ \ln(1 - \beta(1-Q)) - \frac{\beta Q}{1 - \beta(1-Q)} + \ln \left[ \frac{\beta(1-q)}{2\pi} \right] + \frac{1}{K} \ln \left( \frac{1 + (K-1)q}{1-q} \right) \right]. \quad (\text{A14})$$

and finally, neglecting irrelevant constant terms, the expression for the Free Energy reads

$$F[Q, r, x_1, \dots, x_K] = \frac{1}{2} (1-q) \sum_{\alpha=1}^K (x_\alpha)^2 + \frac{1}{2} q \left( \sum_{\alpha=1}^K x_\alpha \right)^2 + \frac{1}{2} \alpha \beta r (1-Q)$$

$$- \frac{1}{\beta} \int \mathcal{D}z \left\langle \left\langle \ln \left[ 2 \cosh \left[ \beta \left( \sum_{\alpha=1}^K \zeta^\alpha x_\alpha + \sqrt{\alpha r} z \right) \right] \right] \right\rangle \right\rangle_\zeta$$

$$+ \frac{\alpha}{2\beta} \left[ \ln[1 - \beta(1-Q)] - \frac{\beta Q}{1 - \beta(1-Q)} \right]. \quad (\text{A15})$$

In the second line, the disorder is to be treated as a random walk, with the "steps"  $\zeta$  distributed according to  $P(\zeta^\alpha = x) = \frac{1+\rho}{2} \delta(x-1) + \frac{1-\rho}{2} \delta(x+1)$ , and the average computation is detailed in section E. Taking the derivatives over  $x_\alpha$ ,  $Q$  and  $r$  we obtain the corresponding saddle point equations:

$$(1-q)x_\alpha + q \left( \sum_{\alpha'=1}^K x_{\alpha'} \right) (= m^\alpha) = \int \mathcal{D}z \left\langle \left\langle \zeta^\alpha \tanh \left( \beta \left[ \left( \sum_{\alpha=1}^K \zeta^\alpha x_\alpha \right) + \sqrt{\alpha r} z \right] \right) \right\rangle \right\rangle_\zeta$$

$$r = \frac{Q}{\left( 1 - \beta(1-Q) \right)^2}$$

$$(1-Q) = \int \mathcal{D}z \left\langle \left\langle \cosh^{-2} \left( \beta \left[ \left( \sum_{\alpha=1}^K \zeta^\alpha x_\alpha \right) + \sqrt{\alpha r} z \right] \right) \right\rangle \right\rangle_\zeta \quad (\text{A16})$$

The main text reports the analysis of the solutions to this set of equations, under the additional symmetry assumption  $x_2 = x_3 = \dots = x_K$ , while  $x_1$  is free. Once the values of  $x_1$  and  $x_2$  are found, the archetype overlaps in the RS approximation are given by

$$O = \int \mathcal{D}z \left\langle \left\langle \eta \tanh \left( \beta \left[ \left( \sum_{\alpha=1}^K \xi^\alpha x_\alpha \right) + \sqrt{\alpha r} z \right] \right) \right\rangle \right\rangle_{\eta, \xi^1, \dots, \xi^K} \quad (\text{A17})$$

## B. Zero Temperature Replica Symmetric Free Energy

In the  $T \rightarrow 0$  limit, one can easily see that:

$$\begin{aligned} \lim_{\beta \rightarrow \infty} \left\{ \tanh(\beta t) \right\} &= \text{sign}(t) \\ \lim_{\beta \rightarrow \infty} \left\{ \frac{\beta}{2} \cosh^{-2}(t) \right\} &= \delta(t) \end{aligned} \quad (\text{B1})$$

Then, introducing the notation  $\beta(1 - Q) = C$  and noting that in the limit  $\beta \rightarrow \infty$   $Q \rightarrow 1$ , from eq. (A16) we get:

$$\begin{aligned} (1 - q) x_\alpha + q \left( x_1 + \sum_{\alpha'=2}^K x_{\alpha'} \right) &= \left\langle \left\langle \zeta^\alpha \text{erf} \left( \frac{1}{\sqrt{2\alpha r}} \left[ \sum_{\alpha'=1}^K \zeta^{\alpha'} x_{\alpha'} \right] \right) \right\rangle \right\rangle_\zeta \\ r &= \frac{1}{(1 - C)^2} \\ C &= \sqrt{\frac{2}{\pi \alpha r}} \left\langle \left\langle \exp \left\{ -\frac{1}{2\alpha r} \left[ \sum_{\alpha'=1}^K \zeta^{\alpha'} x_{\alpha'} \right]^2 \right\} \right\rangle \right\rangle_\zeta \end{aligned} \quad (\text{B2})$$

where  $\text{erf}(x)$  is the error function  $\text{erf}(x) = \frac{2}{\sqrt{\pi}} \int_0^x dz \exp(-z^2)$ .

## C. Finite Temperature 1RSB Free Energy

As for the case of the RS Free Energy, the computation of the 1RSB approximation of our model follows very closely the standard Hopfield's model computation, see for example [17, 18]. Starting from eqs. (A8) to (A10), we now consider the 1RSB structure of the overlap matrix

$$\begin{aligned} \mathbf{Q} &= (1 - q_1) \mathbb{I}_n + (q_1 - q_0) \mathbb{I}_{\frac{n}{m}} \otimes \mathbf{e}_m \mathbf{e}_m^T + q_0 \mathbf{e}_n \mathbf{e}_n^T \\ \mathbf{s} &= (1 - s_1) \mathbb{I}_n + (s_1 - s_0) \mathbb{I}_{\frac{n}{m}} \otimes \mathbf{e}_m \mathbf{e}_m^T + s_0 \mathbf{e}_n \mathbf{e}_n^T, \end{aligned} \quad (\text{C1})$$

where  $\mathbb{I}_n$  denotes an  $n$ -dimensional identity matrix and  $\mathbf{e}_m$  is an  $m$ -dimensional column vector of ones, so that  $\mathbf{e}_m \mathbf{e}_m^T$  is a  $m \times m$  matrix of ones. In the limit  $n \rightarrow 0$ , the variable  $m$  gets promoted to a real variable  $0 \leq m \leq 1$ . After changing variables  $s = \frac{i}{2} \alpha \beta^2 r$ , we obtain:

$$\lim_{n \rightarrow 0} \frac{1}{n} \ln [\tilde{\mathcal{Z}}_{n,K}(r; \{x_\alpha\})] = \int \mathcal{D}z \left\langle \left\langle \log \int \mathcal{D}\tilde{z} \left[ 2 \cosh \left( \beta \left( \sum_{\alpha=1}^K \zeta^\alpha x_\alpha + \sqrt{\alpha r_0} z + \sqrt{\alpha(r_1 - r_0)} \tilde{z} \right) \right) \right]^m \right\rangle \right\rangle_\zeta \quad (\text{C2})$$

$$\begin{aligned} \lim_{n \rightarrow 0} \frac{1}{n} \ln [\tilde{I}_{n,K}(Q)] &= -\frac{1}{2} K \left[ \left( 1 - \frac{1}{m} \right) \log(1 - \beta + \beta q_1) + \frac{1}{m} \log \left( 1 - \beta + \beta (mq_0 + (1 - m)q_1) \right) \right. \\ &\quad \left. - \frac{\beta q_0}{1 - \beta + \beta (mq_0 + (1 - m)q_1)} \right] \end{aligned} \quad (\text{C3})$$

Finally, the expression for the Free Energy as a function of the order parameters reads

$$\begin{aligned} F[q_0, q_1, r_0, r_1, m, x_1, \dots, x_K] &= \frac{1}{2} (1 - q) \sum_{\alpha=1}^K (x_\alpha)^2 + \frac{1}{2} q \left( \sum_{\alpha=1}^K x_\alpha \right)^2 - \frac{1}{2} \alpha \beta \left( r_1 q_1 (1 - m) + r_0 q_0 m - r_1 \right) \\ &\quad - \frac{1}{\beta m} \int \mathcal{D}z \left\langle \left\langle \log \int \mathcal{D}\tilde{z} \left[ 2 \cosh \left( \sum_{\alpha=1}^K \zeta^\alpha x_\alpha + \sqrt{\alpha r_0} z + \sqrt{\alpha(r_1 - r_0)} \tilde{z} \right) \right]^m \right\rangle \right\rangle_\zeta \\ &\quad + \frac{\alpha}{2\beta} \left[ \left( 1 - \frac{1}{m} \right) \log(1 - \beta + \beta q_1) + \frac{1}{m} \log \left( 1 - \beta + \beta (mq_0 + (1 - m)q_1) \right) \right. \\ &\quad \left. - \frac{\beta q_0}{1 - \beta + \beta (mq_0 + (1 - m)q_1)} \right]. \end{aligned} \quad (\text{C4})$$

In the second line, the disorder is to be treated as a random walk, with the "steps"  $\zeta$  distributed according to  $P(\zeta^\alpha = x) = \frac{1+\rho}{2}\delta(x-1) + \frac{1-\rho}{2}\delta(x+1)$ , and the average computation is detailed in section E. As usual, the dominant values of the order parameters are zeroes of the derivatives of  $F$  w.r.t.  $x_\alpha$ ,  $q_0, q_1, r_0, r_1$  and  $m$ , and can be solved numerically. The saddle point equations read

$$\begin{aligned}
(1-q)x_\alpha + q\left(\sum_{\alpha'=1}^K x_{\alpha'}\right) (= m^\alpha) &= \left\langle \left\langle \zeta^\alpha \int \mathcal{D}z \frac{\int \mathcal{D}\tilde{z} \cosh^m \tanh}{\int \mathcal{D}\tilde{z} \cosh^m} \right\rangle \right\rangle_\zeta \\
r_0 &= \frac{q_0}{\left(1 - \beta + \beta(mq_0 + (1-m)q_1)\right)^2} \\
r_1 &= r_0 + \frac{q_1 - q_0}{\left(1 - \beta(1 - q_1)\right)\left(1 - \beta + \beta(mq_0 + (1-m)q_1)\right)} \\
q_0 &= \left\langle \left\langle \int \mathcal{D}z \left[ \frac{\int \mathcal{D}\tilde{z} \cosh^m \tanh}{\int \mathcal{D}\tilde{z} \cosh^m} \right]^2 \right\rangle \right\rangle_\zeta \\
q_1 &= \left\langle \left\langle \int \mathcal{D}z \frac{\int \mathcal{D}\tilde{z} \cosh^m \tanh^2}{\int \mathcal{D}\tilde{z} \cosh^m} \right\rangle \right\rangle_\zeta \\
m &= \frac{2}{\alpha\beta} \frac{\left\langle \left\langle \int \mathcal{D}z \frac{\int \mathcal{D}\tilde{z} \cosh^m \log(\cosh^m)}{\int \mathcal{D}\tilde{z} \cosh^m} \right\rangle \right\rangle_\zeta - \left\langle \left\langle \int \mathcal{D}z \log \int \mathcal{D}\tilde{z} \cosh^m \right\rangle \right\rangle_\zeta}{\frac{q_0}{1 - \beta(1 - q_1 + m(q_1 - q_0))} - \frac{q_1}{1 - \beta(1 - q_1)} + \frac{1}{\beta m} \log \left( \frac{1 - \beta(1 - q_1)}{1 - \beta(1 - q_1 + m(q_1 - q_0))} \right)}
\end{aligned} \tag{C5}$$

where we have used the short-hand notation

$$\begin{aligned}
\cosh &:= \cosh \left( \beta \left( \sum_{\alpha=1}^K \zeta^\alpha x_\alpha + \sqrt{\alpha r_0} z + \sqrt{\alpha(r_1 - r_0)} \tilde{z} \right) \right) \\
\tanh &:= \tanh \left( \beta \left( \sum_{\alpha=1}^K \zeta^\alpha x_\alpha + \sqrt{\alpha r_0} z + \sqrt{\alpha(r_1 - r_0)} \tilde{z} \right) \right)
\end{aligned} \tag{C6}$$

The corresponding free energies is obtained by evaluating  $F[\cdot]$  on the saddle point equations solutions.

#### D. Zero Temperature 1RSB Free Energy

In the  $T \rightarrow 0$  limit, as in the Hopfield model, one has  $D := \beta m$  finite,  $\delta q_1 := (1 - q_1)/T$  finite, and  $[\cosh(\beta x)]^m \rightarrow \exp(D|x|)$ . It follows that, in this limit

$$\begin{aligned}
F[q_0, \delta q_1, r_0, r_1, m, x_1, \dots, x_K] &= \frac{1}{2}(1-q) \sum_{\alpha=1}^K (x_\alpha)^2 + \frac{1}{2}q \left( \sum_{\alpha=1}^K x_\alpha \right)^2 - \frac{1}{2}\alpha \left( D(r_0 q_0 - r_1) - r_1 \delta q_1 \right) \\
&\quad + \frac{\alpha}{2D} \log \left( 1 - \frac{D(1 - q_0)}{1 - \delta q_1} \right) - \frac{1}{2} \frac{\alpha q_0}{1 - \delta q_1 - D(1 - q_0)} \\
&\quad - \frac{1}{D} \left\langle \left\langle \int \mathcal{D}z \log \int \mathcal{D}\tilde{z} \exp \left( D \left| \sum_{\alpha=1}^K \zeta^\alpha x_\alpha + \sqrt{\alpha r_0} z + \sqrt{\alpha(r_1 - r_0)} \tilde{z} \right| \right) \right\rangle \right\rangle_\zeta
\end{aligned} \tag{D1}$$

In the last line of eq. (D1), the innermost integral is a combination of error functions. The corresponding  $T \rightarrow 0$  saddle point equations are obtained by setting to zero the partial derivatives w.r.t.  $q_0, \delta q_1, r_0, r_1, m, x_\alpha$ , and can be

solved numerically. They read:

$$\begin{aligned}
(1 - q) x_\alpha + q \left( \sum_{\alpha'=1}^K x_{\alpha'} \right) &= \left\langle \left\langle \int \mathcal{D}z \zeta^\alpha \frac{I_2}{I_1} \right\rangle \right\rangle_\zeta \\
r_0 &= \frac{q_0}{1 - \delta q_1 - D(1 - q_0)} \\
r_1 &= r_0 + \frac{1 - q_0}{(1 - \delta q_1)(1 - \delta q_1 - D(1 - q_0))} \\
\delta q_0 &= \left\langle \left\langle \int \mathcal{D}z \left( \frac{I_2}{I_1} \right)^2 \right\rangle \right\rangle_\zeta \\
\delta q_1 &= \frac{\sqrt{2}}{\sqrt{\pi} B} \left\langle \left\langle \int \mathcal{D}z \exp \left( -\frac{A^2}{2} \right) \frac{1}{I_1} \right\rangle \right\rangle_\zeta \\
D &= \frac{2}{\alpha} \frac{\left\langle \left\langle \int \mathcal{D}z \frac{I_3}{I_1} \right\rangle \right\rangle_\zeta - \left\langle \left\langle \int \mathcal{D}z \log I_1 \right\rangle \right\rangle_\zeta}{\frac{q_0}{1 - \delta q_1 - D(1 - q_0)} - \frac{1}{1 - \delta q_1} + \frac{1}{D} \log \left( \frac{1 - \delta q_1}{1 - \delta q_1 - D(1 - q_0)} \right)}
\end{aligned} \tag{D2}$$

where

$$\begin{aligned}
I_1 &= \int \mathcal{D}\tilde{z} \exp(DB|A + \tilde{z}|) \\
I_2 &= \int \mathcal{D}\tilde{z} \exp(DB|A + \tilde{z}|) \text{sign}(DB(A + \tilde{z})) \\
I_3 &= \int \mathcal{D}\tilde{z} \exp(DB|A + \tilde{z}|) DB|(A + \tilde{z})|
\end{aligned} \tag{D3}$$

and

$$\begin{aligned}
A &= \frac{z\sqrt{\alpha r_0} + \sum_{\alpha'=1}^K \zeta^{\alpha'} x_{\alpha'}}{\sqrt{\alpha(r_1 - r_0)}} \\
B &= \sqrt{\alpha(r_1 - r_0)}
\end{aligned} \tag{D4}$$

The integrals in eq. (D3) result in combinations of error functions.

### E. How to average over disorder

A crucial part of the analysis consists in averaging over the quenched disorder. This procedure can be carried out in the same way both within the replica-symmetric approximation and within the one-step replica symmetry breaking scheme. Averaging over the quenched disorder proceeds in two steps. We first performed the average over the variables  $\eta$ , as they can be integrated out exactly. This step yields an effective description in which the disorder appears only through the variables  $\zeta$ , as in eqs. (A15) and (C4). Assuming that  $x_2 = x_3 = \dots = x_K$  as in the main text, we have to compute averages of the three kinds:  $\langle g(\sum_{\alpha=1}^K \zeta^\alpha x_\alpha) \rangle$ ;  $\langle \zeta^1 g(\sum_{\alpha=1}^K \zeta^\alpha x_\alpha) \rangle$  and  $\langle \zeta^2 g(\sum_{\alpha=1}^K \zeta^\alpha x_\alpha) \rangle$ , where  $g$  is a scalar function arising from the single-site effective measure. It is convenient to rewrite the sum in the following way

$$\sum_{\alpha=1}^K \zeta^\alpha x_\alpha = (x_1 \zeta^1 + x_2 \zeta^2 + x_2 B_K) \tag{E1}$$

where  $B_K = \sum_{\alpha=3}^K \zeta^\alpha$  collects the contribution of the remaining  $K - 2$  disorder variables and represents a biased random walk of length  $K - 2$ . By construction,  $B_K$  is statistically independent of  $\zeta^1$  and  $\zeta^2$ . With this decomposition, the original high-dimensional quenched average over the  $K$  disorder variables  $\{\zeta^\alpha\}$  is reduced to a finite sum over the configurations of  $(\zeta^1, \zeta^2)$ , combined with an average over the collective random-walk variable  $B_K$ .

As an example, let's focus on  $\langle g(\sum_{\alpha=1}^K \zeta^\alpha x_\alpha) \rangle$ . We first perform the sum over the four possible realizations of  $(\zeta^1, \zeta^2)$ :

$$\begin{aligned}
\langle g(x_1 \zeta^1 + x_2 \zeta^2 + x_2 B_K) \rangle &= p^2 \langle g(x_1 + x_2 + x_2 B_K) \rangle_{B_K} \\
&+ p(1 - p) (\langle g(x_1 - x_2 + x_2 B_K) \rangle_{B_K} + \langle g(-x_1 + x_2 + x_2 B_K) \rangle_{B_K}) \\
&+ (1 - p)^2 \langle g(-x_1 - x_2 + x_2 B_K) \rangle_{B_K}
\end{aligned} \tag{E2}$$

where the symbol  $\langle \dots \rangle_{B_K}$  denotes averaging over realizations of  $B_K$ . Averaging over the random walk we have

$$\langle g(x_1 + x_2 + x_2 B_K) \rangle_{B_K} = \frac{(1-p)^{K-1}}{p} \sum_{X=-(K-2)}^{K-2} \binom{K-2}{\frac{X+K}{2}-1} \left(\frac{p}{1-p}\right)^{(X+K)/2} g(x_1 + x_2 + x_2 X) \quad (\text{E3})$$

where the sum is constrained to  $X$  with the same parity of  $K$ . In the case of  $K$  even,  $K = 2k$  and  $X = 2n$ .

$$\langle g(x_1 + x_2 + x_2 B_K) \rangle_{B_K} = (p(1-p))^{k-1} \sum_{n=-k+1}^{k-1} \binom{2k-2}{n+k-1} \left(\frac{p}{1-p}\right)^n g(x_1 + x_2 + 2x_2 n). \quad (\text{E4})$$

Analogous expressions hold for the other three terms in eq. (E2), and finally

$$\begin{aligned} \langle g(x_1 \zeta^1 + x_2 \zeta^2 + x_2 B_K) \rangle &= \sum_{n=-k+1}^{k-1} A_p(k, n) g(x_1 + x_2 + 2x_2 n) \\ &+ \sum_{n=-k+1}^{k-1} B_p(k, n) g(x_1 - x_2 + 2x_2 n), \end{aligned} \quad (\text{E5})$$

where

$$\begin{aligned} A_p(k, n) &= (p(1-p))^k \left[ \left(\frac{p}{1-p}\right)^{n+1} + \left(\frac{1-p}{p}\right)^{n+1} \right] \binom{2k-2}{n+k-1}, \\ &= 2(p(1-p))^k \cosh\left((n+1) \ln\left(\frac{p}{1-p}\right)\right) \binom{2k-2}{n+k-1}, \\ B_p(k, n) &= (p(1-p))^k \left[ \left(\frac{p}{1-p}\right)^n + \left(\frac{1-p}{p}\right)^n \right] \binom{2k-2}{n+k-1} \\ &= 2(p(1-p))^k \cosh\left(n \ln\left(\frac{p}{1-p}\right)\right) \binom{2k-2}{n+k-1}. \end{aligned} \quad (\text{E6})$$

Analogous expressions hold for  $\langle \zeta^1 g(\sum_{\alpha=1}^K \zeta^\alpha x_\alpha) \rangle$  and  $\langle \zeta^2 g(\sum_{\alpha=1}^K \zeta^\alpha x_\alpha) \rangle$ .